Supporting Information for "A synthesis of upper ocean geostrophic kinetic energy spectra from a global submesoscale permitting simulation"

Hemant Khatri[1], Stephen M. Griffies[1,2], Takaya Uchida[3], Han Wang[4],

Dimitris Menemenlis[5]

[1]Atmospheric and Oceanic Sciences Program, Princeton University, Princeton, New Jersey, USA

[2]NOAA Geophysical Fluid Dynamics Laboratory, Princeton, New Jersey, USA

[3]Institut des Géosciences de l'Environnment, Centre National de la Recherche Scientifique, Grenoble, France

[4]Department of Physics, University of Toronto, Toronto, Canada

[5]Jet Propulsion Laboratory, California Institute of Technology, Pasadena, California, USA

Contents of this file

1. Text S1 on the details of spectral computations.

2. Text S2 on transition wavenumber estimates.

3. Table S1 on details of the latitude and longitude extent of oceanic regions.

4. Figures S1 shows monthly-averaged geostrophic spectra at 3 m depth.

———

Corresponding author: Hemant Khatri, Atmospheric and Oceanic Sciences Program, 300 Forrestal Road, Sayre Hall, Princeton, NJ 08540-6654, USA. (hkhatri@princeton.edu)

October 31, 2020, 2:07am

5. Figure S2 shows the time series of the mean potential energy and enstrophy.

6. Figure S3 shows monthly-averaged rotational kinetic energy and potential energy spectra in late autumn.

Introduction

The document contains additional text, table and figures to support the results presented in the manuscript.

S1. Horizontal wavenumber spectra computations

We follow the methods from Uchida, Abernathey, and Smith (2017) for computing horizontal wavenumber spectra. We compute spectra of kinetic energy (KE) and potential energy (PE) for each model snapshot and used time-averaged spectra for the analysis. In particular, two-dimensional (2D) discrete Fourier transform along both horizontal directions of the velocity and buoyancy fields can be computed first to obtain 2D spectra of KE, $E(k_x, k_y)$, and PE, $P(k_x, k_y)$,

$$E(k_x, k_y) = \frac{1}{2\Delta k_x \Delta k_y} |\tilde{\mathbf{u}}(k_x, k_y)|^2, \tag{1}$$

$$P(k_x, k_y) = \frac{1}{2\Delta k_x \Delta k_y} \frac{|\tilde{b}(k_x, k_y)|^2}{N^2}, \tag{2}$$

where $\mathbf{k} = (k_x, k_y)$ is the horizontal wavenumber vector, and $\Delta k_x = 1/(2\Delta x)$, $\Delta k_y = 1/(2\Delta y)$ (Δx and Δy are the zonal and meridional grid spacings) are the inverse of the smallest wavelengths admitted by the model grid. $\tilde{\mathbf{u}}(k_x, k_y)$ and $\tilde{b}(k_x, k_y)$ are the 2D Fourier transform of the velocity and buoyancy ($b = -g(\rho - \rho_o)/\rho_o$, where $g = 9.8$ m/s^2, ρ is the potential density referenced to the ocean surface, $\rho_o = 1000$ kg/m^3 is the reference density). N is the buoyancy frequency ($N^2 = -(g/\rho_o)\,\mathrm{d}\rho(z)/\mathrm{d}z$, where

$\rho(z)$ represents the spatial and time mean vertical potential density profile). Potential density was evaluated using the equation of state from Jackett and Mcdougall (1995). Prior to Fourier transform computations, spatial linear trends were removed from each data snapshot and a 2D Planck-taper windowing function ($\exp[-\frac{0.01}{1-x^2} - \frac{0.01}{1-y^2} + 0.02]$, where $(x, y) \epsilon [-1, 1]$) was used to make the fields doubly-periodic. Planck-taper window is quite effective in reducing signal leakage (McKechan et al., 2010). Alternatively, a Hanning window (or other windowing operations) can be used for this purpose (see e.g. Rocha, Gille, Chereskin, and Menemenlis (2016)).

A Helmholtz decomposition can be used to obtain the KE spectra corresponding to the rotational and divergent components of the horizontal flow (Bühler et al., 2014; Uchida et al., 2017). Decomposing the horizontal velocity, $\mathbf{u}$, in terms of a streamfunction, ψ, and velocity potential, ϕ, yields

$$\mathbf{u} = \mathbf{u}_\psi + \mathbf{u}_\phi = \hat{\mathbf{z}} \times \nabla\psi + \nabla\phi, \tag{3}$$

$$\zeta = \hat{\mathbf{z}} \cdot (\nabla \times \mathbf{u}) = \nabla^2\psi, \tag{4}$$

$$\mathcal{D} = \nabla \cdot \mathbf{u} = \nabla^2\phi, \tag{5}$$

where ζ and $\mathcal{D}$ are the vertical components of the relative vorticity and horizontal divergence, respectively. In Fourier space, the above relations take the form

$$\tilde{\zeta} = -(k_x^2 + k_y^2)\tilde{\psi} \qquad \text{and} \qquad \tilde{\mathcal{D}} = -(k_x^2 + k_y^2)\tilde{\phi}. \tag{6}$$

We can then use these equations to compute rotational (K^ψ) and divergent (K^ϕ) components of the KE spectra ($E = K^\psi + K^\phi$) as

$$K^\psi = \frac{1}{2}|\tilde{\mathbf{u}}_\psi|^2 = \frac{|\tilde{\zeta}|^2}{2(k_x^2 + k_y^2)}, \tag{7}$$

$$K^\phi = \frac{1}{2}|\tilde{\mathbf{u}}_\phi|^2 = \frac{|\tilde{\mathcal{D}}|^2}{2(k_x^2 + k_y^2)}. \tag{8}$$

In this paper, we azimuthally integrate the 2D spectra to obtain spectra as a function of the isotropic wavenumber, $k = (k_x^2 + k_y^2)^{1/2}$.

S2. Comparing the transition wavenumber estimate against other studies

Tulloch and Smith (2006) studied the coexistence of quasi-geostrophic (QG) and surface-QG turbulence by incorporating both interior and boundary dynamics in an idealized model. They observed the change in spectral scaling from k^{-3} to $k^{-5/3}$ in the surface KE spectrum and defined the corresponding transition wavenumber as $k_T = f/NH$, where f is the Coriolis parameter, N is buoyancy frequency and H is equivalent to thermocline depth.

Our k_T definition in equation (4) in the manuscript agrees with the transition wavenumber estimated by Tulloch and Smith (2006). We see the equivalence by using scaling arguments with $b = f\,\partial\psi/\partial z$ (b is buoyancy and ψ is streamfunction) from geostrophy and $\zeta = k_T^2\psi$ (ζ is the relative vorticity), thus yielding

$$k_T = \frac{f}{NH} = \frac{f}{N}\sqrt{\frac{\langle\psi^2\rangle}{H^2}\frac{1}{\langle\psi^2\rangle}}, \tag{9}$$

$$k_T \approx \frac{f}{N}\sqrt{\langle|\frac{\partial\psi}{\partial z}|^2\rangle\frac{1}{\langle\psi^2\rangle}} \approx \frac{1}{N}\sqrt{\frac{\langle b^2\rangle}{\langle\zeta^2\rangle}k_T^4}, \tag{10}$$

$$k_T \approx \sqrt{\frac{N^2\langle\zeta^2\rangle}{\langle b^2\rangle}}. \tag{11}$$

References

October 31, 2020, 2:07am

Bühler, O., Callies, J., & Ferrari, R. (2014). Wave-vortex decomposition of one-dimensional ship-track data. *J. Fluid Mech.*, *756*, 1007-1026. doi: 10.1017/jfm.2014.488

Gkioulekas, E., & Tung, K. K. (2007). Is the subdominant part of the energy spectrum due to downscale energy cascade hidden in quasi-geostrophic turbulence? *Discrete & Continuous Dynamical Systems-B*, *7*(2), 293. doi: 10.3934/dcdsb.2007.7.293

Jackett, D. R., & Mcdougall, T. J. (1995). Minimal adjustment of hydrographic profiles to achieve static stability. *Journal of Atmospheric and Oceanic Technology*, *12*(2), 381–389. doi: 10.1175/1520-0426(1995)012⟨0381:MAOHPT⟩2.0.CO;2

McKechan, D., Robinson, C., & Sathyaprakash, B. S. (2010). A tapering window for time-domain templates and simulated signals in the detection of gravitational waves from coalescing compact binaries. *Classical and Quantum Gravity*, *27*(8), 084020. doi: 10.1088/0264-9381/27/8/084020

Rocha, C. B., Gille, S. T., Chereskin, T. K., & Menemenlis, D. (2016). Seasonality of submesoscale dynamics in the kuroshio extension. *Geophysical Research Letters*, *43*(21), 11–304. doi: 10.1002/2016GL071349

Tulloch, R., & Smith, K. (2006). A theory for the atmospheric energy spectrum: Depth-limited temperature anomalies at the tropopause. *Proceedings of the National Academy of Sciences*, *103*(40), 14690–14694. doi: 10.1073/pnas.0605494103

Uchida, T., Abernathey, R., & Smith, S. (2017). Seasonality of eddy kinetic energy in an eddy permitting global climate model. *Ocean Modell.*, *118*, 41–58. doi: 10.1016/j.ocemod.2017.08.006

Table S1.   Latitude and longitude bands of different regions. Acronyms for high and relatively

low KE regions start with 'H' and 'L', respectively.

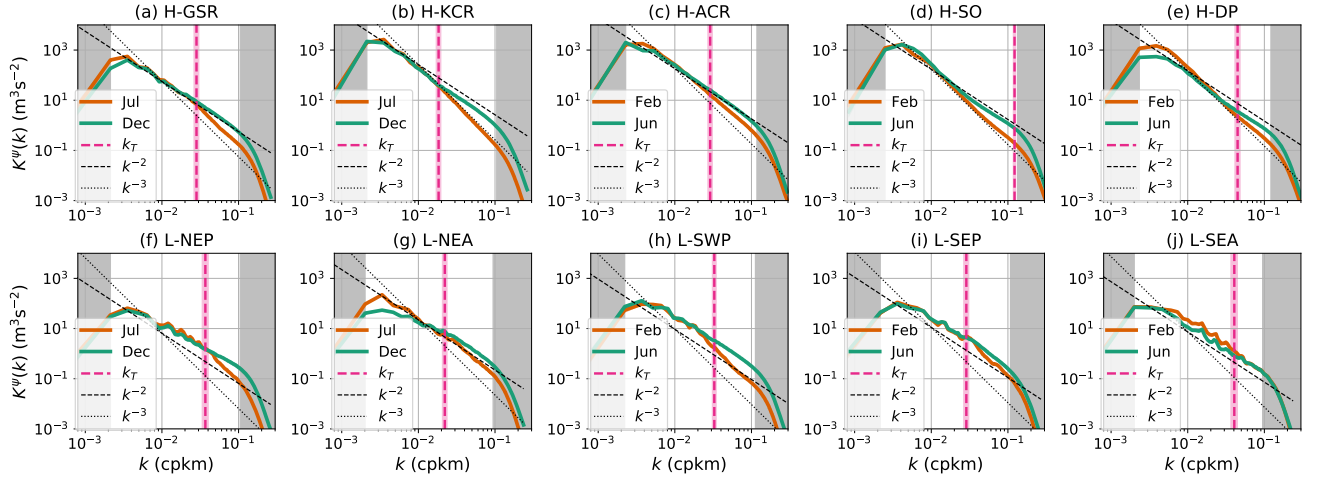| Acronyms	Latitudinal Extent	Longitudinal Extent	Location
H–GSR	30°N − 40°N	55°W − 45°W	Gulf Stream Region
H–KCR	30°N − 40°N	150°E − 160°E	Kuroshio Current Region
H–ACR	48°S − 38°S	20°E − 30°E	Agulhus Current Region
H–SO	55°S − 45°S	120°E − 130°E	Southern Ocean
H–DP	50°S − 40°S	50°W − 40°W	Drake Passage Region
L–NEP	30°N − 40°N	150°W − 140°W	North East Pacific
L–NEA	19°N − 29°N	38°W − 28°W	North East Atlantic
L–SWP	45°S − 35°S	150°W − 140°W	South West Pacific
L–SEP	42°S − 32°S	100°W − 90°W	South East Pacific
L–SEA	30°S − 30°S	10°W − 0°W	South East Atlantic

Figure S1. Monthly-averaged rotational KE spectra versus isotropic horizontal wavenumber $k = \sqrt{k_x^2 + k_y^2}$ at 2.79 m depth in different regions. k_T is the transition wavenumber computed using the relation in equation 1 (computed using Dec month data in (a, b, f, g) and June month data in (c-e, h-j)) and shading represents the standard deviation. k^{-2} and k^{-3} curves are shown with dashed and dotted black lines, respectively. Gray regions indicate the wavenumbers over which boundary effects (low wavenumbers) and viscous dissipation (high wavenumbers) significantly alter the spectra, so are outside our scope. Unlike in the manuscript, we show spectra computed for the months of Dec (a, b, f, g) and June (c-e, h-j) because we only computed spectra for DJF and JJA seasons at 2.79 m depth level to limit the computational expense. Nevertheless, dual spectral inertial ranges are evident, which indicates the coexistence of QG turbulence and frontal-surface-QG turbulence.
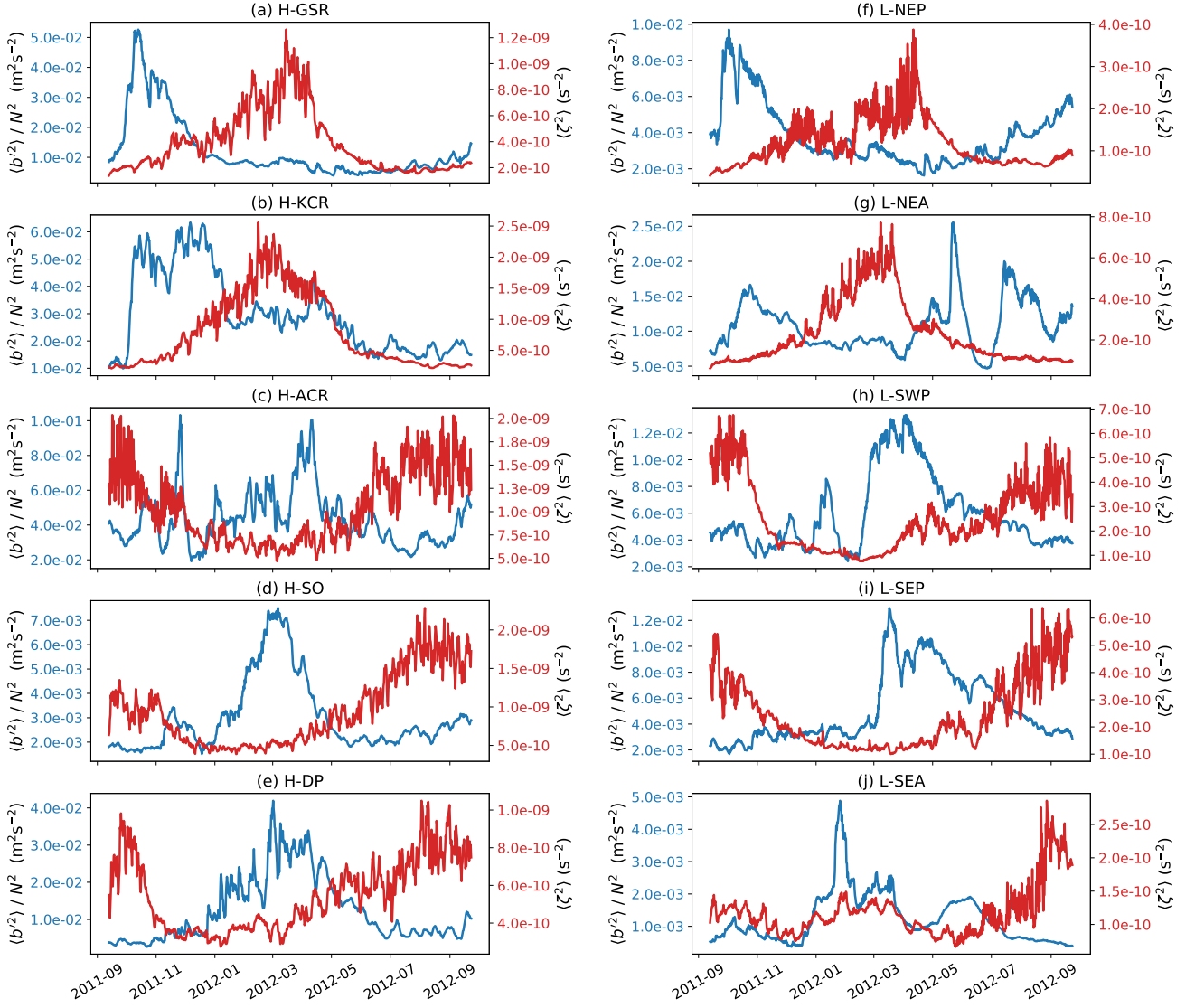
Figure S2. Time series of domain-averaged available potential energy (blue) and domain-averaged enstrophy (red) at 21 m depth in different regions. There is a lag of about 2-4 months in the peaks of available potential energy and enstrophy in all regions.
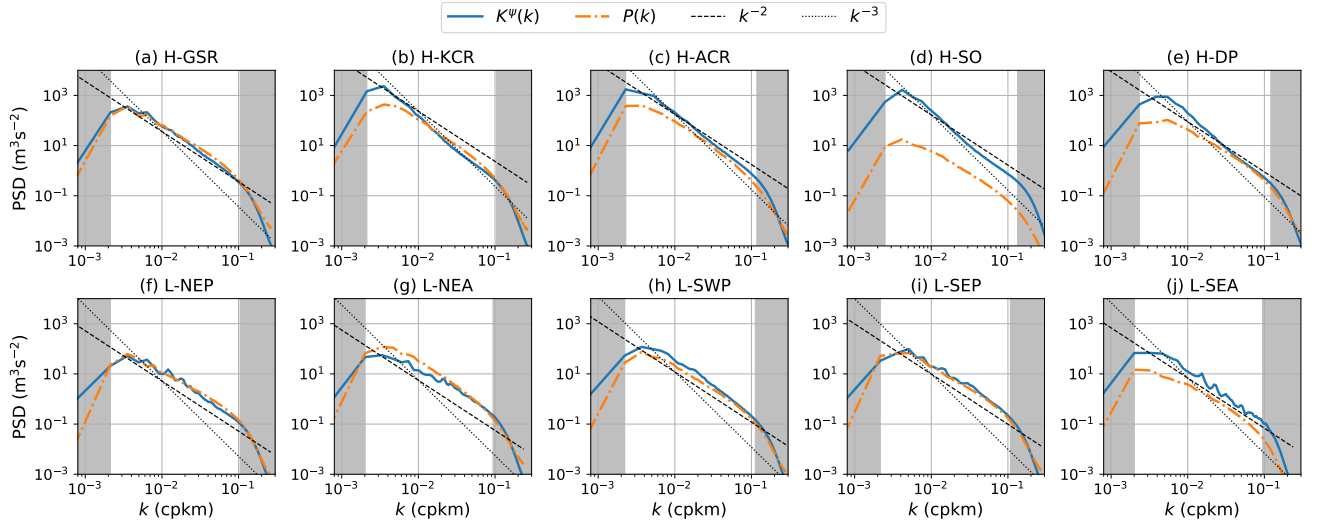
Figure S3. Monthly-averaged rotational kinetic energy ($K^\psi(k)$) and potential energy ($P(k)$) spectra in late autumn at 21 m depth in different regions. Spectra shown are for the month of Nov in (a, b, f, g) and for the month of May in (c-e, h-j). k^{-2} and k^{-3} curves are shown with dashed and dotted black lines, respectively. Gray regions indicate the wavenumbers over which boundary effects (low wavenumbers) and viscous dissipation (high wavenumbers) significantly alter the spectra, so are outside our scope. At length scales larger than about 50 km, $K^\psi(k)$ follows close to k^{-3} scaling. At length scales smaller than about 50 km, the spectral slope in $K^\psi(k)$ is relatively shallow, $\sim k^{-2}$, due to pronounced frontal-surface-QG behavior (see the description of figure 3 in the manuscript). In high KE regions, at these scales (< 50 km), $K^\psi(k)$ and $P(k)$ are of similar magnitudes with similar power-law scaling, and this energy equipartition is expected in surface-QG dynamics (Gkioulekas & Tung, 2007). However, the energy equipartition condition is not satisfied in the H–SO region (k_T estimate also does not match the wavenumber corresponding to the spectral scaling change in this region, see manuscript).